± 5.0% of EGFP-positive cells, and 87.3% ± 2.6% of Iba1-positive cells coexpressed CD68, which also demonstrated that BM-derived cells expressing Iba1 were of macrophage lineage.

Observation of BM-derived cells expressing Iba1 in the cochlea with a confocal microscope revealed a specific morphological feature that was characterized by a spindle shape with several ramified processes, a characteristic morphological feature of macrophages (Fig. 2a–c). In addition to the immunohistochemistry phenotype, BM-derived cells expressing Iba1 in the cochlea morophologically followed microglias that are referred to as resident tissue macrophages in the CNS.

Systemic Application of M-CSF Increased the Number of Iba1-Positive Cells in the Cochlea

To characterize Iba1-positive cells in the cochlea, we next examined the mobilization of Iba1-positive cells using systemic application of M-CSF, the primary regulator of activation of mononuclear phagocytes in wild-type C57BL/6 mice. Iba1-positive cells in both SL and SG were observed more densely in M-CSF-treated mice (Fig. 3a,b) than in controls (Fig. 3c,d). The density of Iba1-positive cells in SL of the middle turn in the controls was 1.46 ± 0.22 (cells/10^4 μm^2), which increased to 2.54 ± 0.45 after M-CSF treatment (Fig. 3e), although the difference was not significant. By contrast, a significant increase was identified in the density of Iba1-positive cells in SG (from 1.39 ± 0.18 to 2.95 ± 0.3; Fig. 3e). These data revealed that Iba1-positive cells in the cochlea are under the control of M-CSF signaling. In addition to the findings of phenotype and morphology, we have demonstrated that BM-derived cells labeled with Iba1 have a quality of resident tissue macrophage in the cochlea.

Cochlear Macrophages Gradually Turn Over for More Than 6 Months

The percentage of chimerism in the peripheral blood at 3 months after BM transplantation was 82.8% ± 3.6%, indicating that hematopoietic reconstitution was performed successfully at this time point. The chimeric ratio observed in the present study was compatible with previous reports on BM chimeric mice (Yoshimoto et al., 2003; Lang et al., 2006). Sequential observation of Iba1-positive cells in the cochlea of transplanted mice demonstrated that cochlear macrophages labeled with Iba1 survived systemic irradiation and were gradually replaced by EGFP-positive cells derived from transplanted HSCs. One or two weeks after HSC transplantation, no EGFP-positive cells were found within cochlear tissues. By contrast, at 4 weeks after transplantation, expression of EGFP was found in 15.4% ± 6.6% of Iba1-positive cells in the cochlea. The ratio for EGFP expression in Iba1-positive cells increased remarkably to 64.9% ± 8.1% in cochlear specimens obtained at 3 months (12 weeks) after transplantation, then reached 84.1% ± 1.6% at 6 months (24 weeks) after transplantation. The differences in the ratio for EGFP expression in Iba1-positive cells were significant at 3 and 6 months compared with 1, 2, or 4 weeks (Fig. 4). The distribution of Iba1-positive cells in the cochlea was identical at each time point (data not shown). The density of Iba1-positive cells in SL was 2.39 ± 0.32 (cells/10^4 μm^2) at

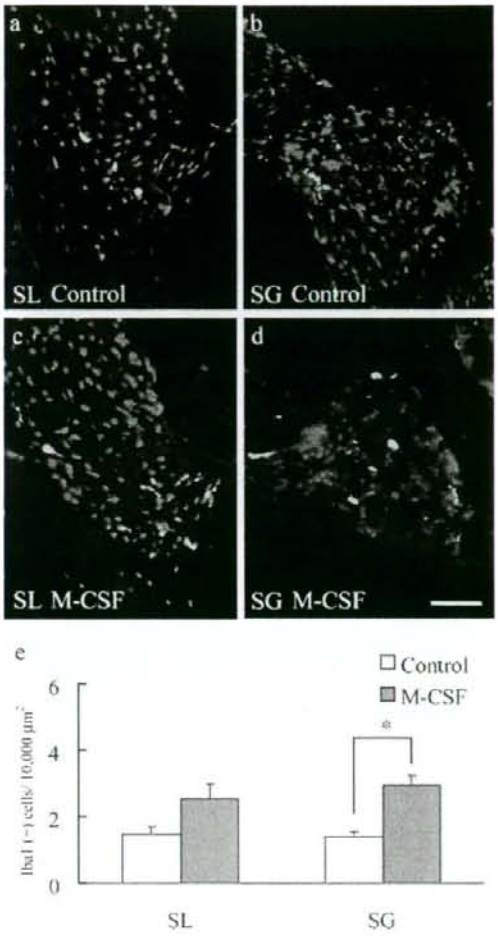

Fig. 3. Systemic application of macrophage colony-stimulating factor increases the density of Iba-1-positive cells in the spiral ligament (SL) and spiral ganglion (SG). **a–d:** Several Iba1-positive cells were found in the SL (c) and the SG (d) following systemic application of macrophage colony-stimulating factor (M-CSF), although few cells expressing Iba1 were observed in control specimens (a,b). **e:** Densities of Iba1-positive cells (cells/10^4 μm^2) in SG of M-CSF-treated cochleae were significantly higher than those of control cochleae (*$P = 0.002$, unpaired t-test), although no significant difference is found in SL ($P = 0.06$). Bars represent standard errors. Scale bar = 50 μm.

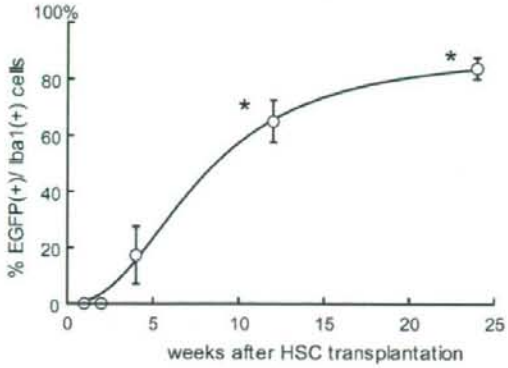

Fig. 4. Sequential analysis of chimeric ratios for Iba1-positive cells following transplantation of hematopoietic stem cells derived from GFP mice. The ratios for EGFP expression in Iba1-positive cells of the whole cochlea are shown at 1, 2, and 4 weeks and 3 (12 weeks) and 6 (24 weeks) months after transplantation. The graph demonstrates a gradual increase in the ratio of EGFP expression in Iba1-positive cells, indicating replacement of native Iba1-positive cells by EGFP-positive cells derived from engrafted hematopoietic stem cells. The ratio at 3 or 6 months is significantly higher than that at 1, 2, or 4 weeks ($*P < 0.001$, ANOVA with Tukey-Kramer's test). Bars show standard errors.

1 week, 2.67 ± 0.07 at 2 weeks, 3.02 ± 0.42 at 4 weeks, 3.25 ± 0.18 at 3 months, and 3.31 ± 0.11 at 6 months after BM transplantation. The density of Iba1-positive cells in SG was 1.35 ± 0.10 (cells/10^4 μm^2) at 1 week, 1.73 ± 0.37 at 2 weeks, 1.22 ± 0.15 at 4 weeks, 1.93 ± 0.32 at 3 months, and 2.26 ± 0.14 at 6 months after BM transplantation. There were no significant differences in the density of Iba1-positive cells in SL among the experimental groups. However, the increase with age in the density of Iba1-positive cells in SG was statistically significant between 1 week and 6 months and between 4 weeks and 6 months. These findings indicate that cochlear macrophages are not eliminated by systemic irradiation and gradually turn over for more than 6 months in nondamaged cochlea.

Cochlear Macrophages Increased in Response to Local Surgical Stress

To examine the reaction of cochlear macrophages to an acute, local, exogenous stress on the cochlea, surgical invasion with application of physiological saline via PSCC was performed on both wild-type and BM chimeric mice. ABR recoding was performed to determine the extent of functional damage following treatment. Significant elevation of ABR thresholds was observed on day 1 after local treatment, whereas no elevation was found on days 7 and 28 at all frequencies (Fig. 5a), indicating that the surgical stress used in the present study caused temporary damage to the cochlea.

Iba1-positive cells were increased temporarily in response to local surgical stress in SL and SG (Fig. 5b–e). The density of Iba1-positive cells in SL exhibited an immediate response to the treatment on day 1 after surgery (3.96 ± 0.16 cells/10^4 μm^2 vs. 1.62 ± 0.18, preoperative), significantly increased on day 7 after surgery (5.42 ± 0.59), and decreased on day 28 (2.90 ± 0.41; Fig. 5f). No significant difference was found in the densities of Iba1-positive cells between before surgery, on day 1, or on day 28. A temporary increase was also found in the density of Iba1-positive cells in SG on day 1 (1.94 ± 0.06) and day 7 (2.66 ± 0.33; Fig. 5f) compared with densities of 1.20 ± 0.09 preoperatively and 1.33 ± 0.16 on day 28. The differences between preoperative values and day 7 and between days 7 and 28 were statistically significant.

We also examined the effect of local surgical stress in BM chimeric mice that had been transplanted with HSCs labeled with EGFP 3 months before, to test the mobilization of Iba1-positive cell from BM to the cochlea. The density of cells dually labeled with EGFP and Iba1 studied in SL at day 7 after treatment was 4.01 ± 0.21 (cells/10^4 μm^2) in the operated group and 2.54 ± 0.39 in nonoperated BM chimeric mice, and that in SG was 1.88 ± 0.52 in the operated group and 1.42 ± 0.21 in the nonoperated group. The difference in the density of EGFP-positive cells in SL between the two groups was statistically significant, whereas that in SG was not significant.

Immunohistochemistry for Ki67 was performed before and at days 1 andf 7 after surgical treatment, to test whether the increase in cochlear macrophages following surgical treatment was due to proliferation in situ. On day 1 following treatment, 1.75 ± 0.85 cells/section were found to be dually labeled with Ki67 and CD68 (1.74 ± 0.71% in total number of cells positive for CD68). On day 7 following treatment, 2.25 ± 0.75 were dually labeled with Ki67 and CD68 (2.49% ± 0.81%), in contrast to 1.00 ± 0.40 in untreated mice (1.53% ± 0.51%). All Ki67-positive cells in the three groups were found in the lower part of SL. However, no statistically significant difference was observed in the number of Ki67-positive cells among the three groups. These findings indicated that the increase in cochlear macrophages was due mainly to the migration of macrophages from the circulation into the cochlea. However, it was also revealed that the proliferation of macrophages in situ is one of the possible sources for cochlear macrophages.

DISCUSSION

The present study revealed that BM-derived cells are supplied continuously to the cochlea even in the adult mouse and demonstrated that the predominant phenotype of macrophages involved expression of CD68, F4/80, or Iba1 in SL and SG. Our study on the morphology, immunohisotochemical phenotype, and reactivity to M-CSF provides evidence that hematopoi-

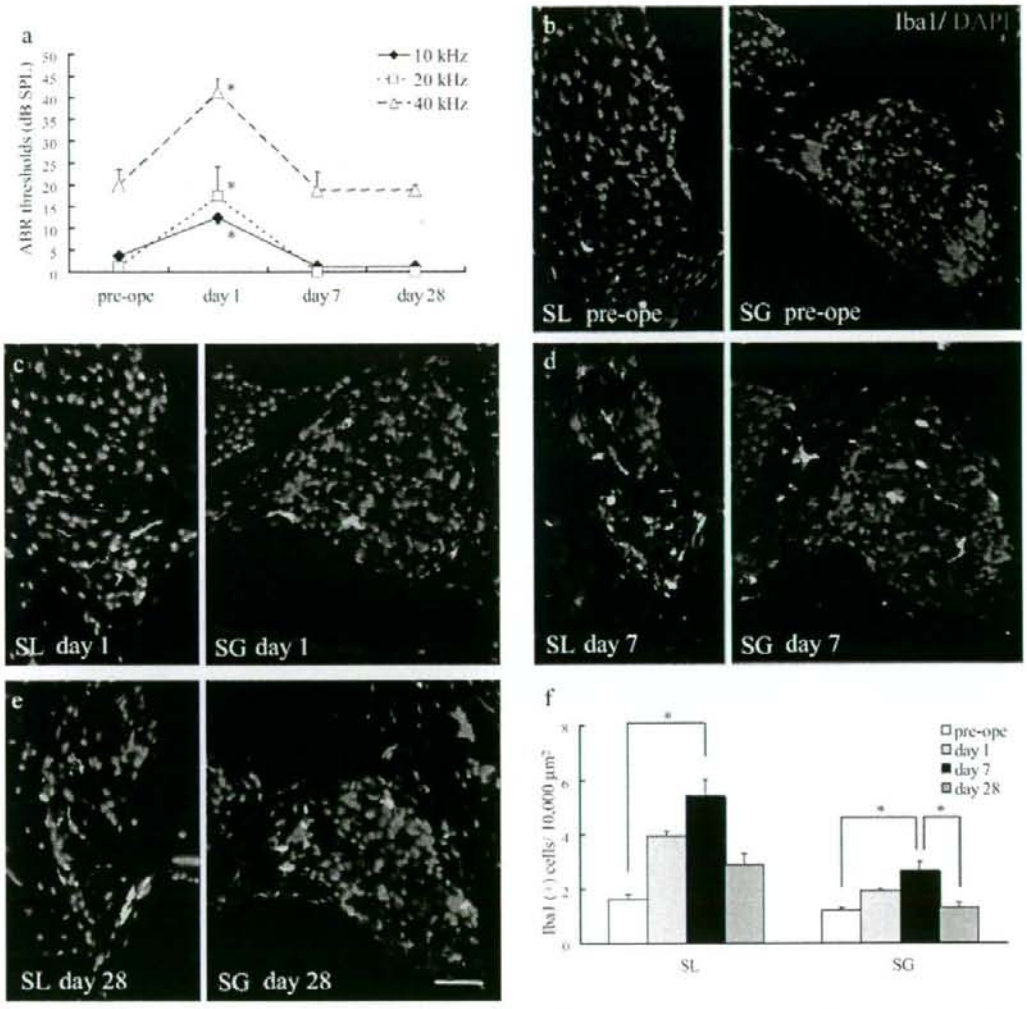

Fig. 5. Effects of local surgical stress on densities of Iba1-positive cells in the spiral ligament (SL) and spiral ganglion (SG). **a:** Local surgical stress causes significant elevation of ABR thresholds at each frequency on day 1 after treatment ($*P < 0.001$, ANOVA with Tukey-Kramer's test), and the elevation recovered on days 7 and 28 at all the frequencies tested. **b–e:** Immunostaining for Iba1 in cochlear specimens obtained preoperatively (pre-ope; b) and on day 1 (c), day 7 (d), and day 28 (e) after treatment. Increase in Iba1-positive cells was observed in the SL and SG of cochleae obtained on days 1 and 7. **f:** The density of Iba1-positive cells (cells/10^4 μm^2) on day 7 was significantly higher than that in preoperative specimens in both SL ($*P = 0.003$) and SG ($*P = 0.002$) or day 28 in SG. Bars show standard errors. Scale bars = 50 μm.

etic BM-derived cells expressing Iba1 are constitutively present as resident tissue macrophages in the cochlea. The examination of the recruitment of cochlear macrophages demonstrated that these cells exhibited slow turnover for several months during steady-state conditions and quickly increased in response to local surgical stress.

Although earlier studies have demonstrated infiltration of inflammatory cells, including macrophages, into the cochlea following inner ear injury (Fredelius, 1988; Bhave et al., 1998; Hirose et al., 2005; Tornabene et al., 2006; Ladrech et al., 2007), two recent studies have suggested the presence of resident tissue macrophages in the inner ear.

Lang et al. (2006) reported that BM-derived cells are constitutively present and widely distributed in the cochlea in the same manner demonstrated in the present study. Although they concluded negatively that only 5% of BM-derived cells differentiated into CD45R-positive macrophages, the rate for CD45 expression in BM-derived cells is also compatible with the present study. The authors instead emphasized that histological analysis of the cochleae following HSCs revealed the contribution of BM-derived cells to fibrocytes or mesenchymal cells in the inner ear. However, the specific ratios for immunoreactivity of Na, K-ATPase, or the Na-K-Cl transporter in the BM-derived cells were not determined in their study. Moreover, there is a discrepancy in the ratio for the expression of F4/80 between the study by Lang et al. (2006) and the present study, although both studies used HSC-transplanted mice that exhibited similar chimeric ratios in peripheral blood and SL cells. One possible explanation for this discrepancy is a difference in methods for immunohistochemistry. We used cryostat sections, whereas Lang et al. used paraffin-embedded sections. Our study demonstrated that more than 80% of BM-derived cells in SL and SG show the phenotype of macrophages and that resident tissue macrophages in the cochlea during steady-state conditions are present in a larger number than reported previously.

Another report was made by Hirose et al. (2005) that CD45-positive mononuclear phagocytes are present in the SL of nonnoise-exposed $CX3CR1^{GFP/GFP}$ transgenic mice, and these cells are also labeled with Iba1 or CD68, which is consistent with the results of the present study. However, the density of CD45-positive cells in the cochlea was quite different between the wild-type and $CX3CR1^{GFP?GFP}$ transgenic mice used in their study, although the number of BM-derived cells expressing CD45 in the cochlea demonstrated in the present study was identical to that of CD45-positive cells in the cochlea of nonnoise-exposed wild-type mice presented by Hirose et al. (2005). The most controversial point is whether it is appropriate to assume that macrophages observed in the cochlea can be described as "microglia-like" cells. Although the authors failed to describe the distribution of macrophages in the auditory nervous system including the SG and cochlear modiolus during steady-state conditions, they distinguish the infiltrating macrophages observed after noise exposure from microglias in the CNS by the morphology and the potentiality of exchanging from the vascular space. The proliferation in situ is thought to be one of the main sources of microglia in adults, but some studies have reported that BM-derived cells can enter the CNS and populate the microglial cell compartment (Lawson et al., 1992; Corti et al., 2002; Hess et al., 2004; Simard and Rivest, 2004; Malm et al., 2005). Moreover, previous studies in the CNS using flow cytometry or immunohistochemistry defined a profile of characterization of microglial cells corresponding to the following phenotype: $CD68^+$, CD45 low, $CD11b^+$, CD11c high, and MHC class II^+ (Guillemin and Brew, 2004; Floden and Combs, 2007). Our results on cochlear resident macrophages "$CD68^+$, $Iba1^+$, and $CD45^-$" were compatible with the immunochemical definition of microglias as reported above. In addition, the cochlear resident macrophages were observed in the auditory nervous system as well as in the connective tissue of SL in the present study. Because there is a considerable heterogeneity in the phenotypes of the macrophage lineage, and because resident tissue macrophages share several antigens with infiltrating macrophages (Guillemin and Brew, 2004), further studies should be carried out to define a profile of characterization on both resident and infiltrating macrophages in the cochlea.

Many studies on resident tissue macrophages in other organs have been performed with BM chimeric mice. In terms of replacement of resident tissue macrophages by BM, donor-derived cells are reported rapidly to populate the liver with Kupffer cells, resident macrophages in the liver, within 3 weeks, and donor Kupffer cells in liver transplants are replaced with similar kinetics (Naito et al., 1997). Microglias in the CNS exhibit longer turnover period than cochlear resident macrophages. At 12 months following HSC transplantation, 40% of microglias have been replaced by hematopoietic cells (Hess et al., 2004; Simard and Rivest, 2004). In contrast, Xu et al. (2007) reported that EGFP-positive BM-derived cells infiltrate normal retina in significant numbers at 8 weeks after BM transplantation and that by 6 months all retinal microglia/macrophges were replaced by BM-derived EGFP-positive cells, the turnover rate of which is very similar to that of the inner ear in the present findings. From the viewpoint of turnover rates, cochlear resident macrophages have characteristics as resident macrophages in the retina.

Although BM chimeric mice are a powerful tool for the analysis of the dynamics of BM-derived cells, there are some limitations. The results of BM chimeric mice are obtained under extraordinary conditions; systemic lethal irradiation and following BM transplantation. It is also technically difficult to set an ideal negative control, with irradiation but without BM transplantation. Moreover, it is difficult to exclude completely the possibility that the results observed in this study are caused by irradiation-induced damage. However, despite these limitations in studies using BM chimeric mice, our results provided some new insights into the origin and distribution of cochlear resident macrophages and the possible supply of cochlear macrophages by replenishment with BM-derived cells.

Recent studies have demonstrated multiple key functions of resident tissue macrophages not only in phagocytosis of foreign bodies or senescent cells but also in the production and secretion of cytokines and the regulation of specific immune responses (Gordon and Taylor, 2005). In the CNS, microglias have both neurotrophic and neurotoxic properties (Kreutzberg, 1996; Moore and Thanos, 1996; Streit, 1996) and play an effector role in both innate and adaptive immune responses, allowing the CNS to respond rapidly and

efficiently to a wide range of pathogens (Olson and Miller, 2004). Although it has not been elucidated whether the infiltrating macrophages play beneficial or harmful roles in the maintenance of auditory function, pharmacological intervention in the infiltration of macrophages may be a possible strategy for treatment of SNHL. In conclusion, the resident cochlear macrophages have potential as a therapeutic target by means of controlling their ability of phagocytosis, migration, or release of cyokines in the pathology of inner ear immune disorders.

ACKNOWLEDGMENTS

The authors thank Dr. Masaru Okabe (Osaka University) for generously providing EGFP transgenic mice and Dr. Junko Okano (Department of Anatomy and Developmental Biology, Graduate School of Medicine, Kyoto University) for critical discussion. We are also very thankful to Dr. Hideaki Ogita, Ms. Yoko Nishiyama, Ms. Rika Sadato, Ms. Akemi Saito, Ms. Keiko Nishio, and Ms. Tomoyo Namura for their excellent technical assistance.

REFERENCES

Bhave SA, Oesterle EC, Coltrera MD. 1998. Macrophage and microglia-like cells in the avian inner ear. J Comp Neurol 398:241–256.

Corti S, Locatelli F, Donadoni C, Strazzer S, Salani S, Del Bo R, Caccialanza M, Bresolin N, Scarlato G, Comi GP. 2002. Neuroectodermal and microglial differentiation of bone marrow cells in the mouse spinal cord and sensory ganglia. J Neurosci Res 70:721–733.

Floden AM, Combs CK. 2007. Microglia repetitively isolated from in vitro mixed glial cultures retain their initial phenotype. J Neurosci Methods 164:218–224.

Fredelius L. 1988. Time sequence of degeneration pattern of the organ of Corti after acoustic overstimulation. A transmission electron microscopy study. Acta Otolaryngol 106:373–385.

Gordon S, Taylor PR. 2005. Monocyte and macrophage heterogeneity. Nat Rev Immunol 5:953–964.

Guillemin GJ, Brew BJ. 2004. Microglia, macrophages, perivascular macrophages, and pericytes: a review of function and identification. J Leukocyte Biol 75:388–397.

Hess DC, Abe T, Hill WD, Studdard AM, Carothers J, Masuya M, Fleming PA, Drake CJ, Ogawa M. 2004. Hematopoietic origin of microglial and perivascular cells in brain. Exp Neurol 186:134–144.

Hirose K, Discolo CM, Keasler JR, Ransohoff R. 2005. Mononuclear phagocytes migrate into the murine cochlea after acoustic trauma. J Comp Neurol 489:180–194.

Iguchi F, Nakagawa T, Tateya I, Kim TS, Endo T, Taniguchi Z, Naito Y, Ito J. 2003. Trophic support of mouse inner ear by neural stem cell transplantation. Neuroreport 14:77–80.

Imai Y, Ibata I, Ito D, Ohsawa K, Kohsaka S. 1996. A novel gene iba1 in the major histocompatibility complex class III region encoding an EF hand protein expressed in a monocytic lineage. Biochem Biophys Res Commun 224:855–862.

Kim TS, Nakagawa T, Kitajiri S, Endo T, Takebayashi S, Iguchi F, Kita T, Tamura T, Ito J. 2005. Disruption and restoration of cell-cell junctions in mouse vestibular epithelia following aminoglycoside treatment. Hear Res 205:201–209.

Kreutzberg GW. 1996. Microglia: a sensor for pathological events in the CNS. Trends Neurosci 19:312–318.

Ladrech S, Wang J, Simonneau L, Puel JL, Lenoir M. 2007. Macrophage contribution to the response of the rat organ of Corti to amikacin. J Neurosci Res 85:1970–1979.

Lang H, Ebihara Y, Schmiedt RA, Minamiguchi H, Zhou D, Smythe N, Liu L, Ogawa M, Schulte BA. 2006. Contribution of bone marrow hematopoietic stem cells to adult mouse inner ear: mesenchymal cells and fibrocytes. J Comp Neurol 496:187–201.

Lawson LJ, Perry VH, Gordon S. 1992. Turnover of resident microglia in the normal adult mouse brain. Neuroscience 48:405–415.

Lee JE, Nakagawa T, Kim TS, Iguchi F, Endo T, Dong Y, Yuki K, Naito Y, Lee SH, Ito J. 2003. A novel model for rapid induction of apoptosis in spiral ganglions of mice. Laryngoscope 113:994–999.

Malm TM, Koistinaho M, Parepalo M, Vatanen T, Ooka A, Karlsson S, Koistinaho J. 2005. Bone-marrow-derived cells contribute to the recruitment of microglial cells in response to beta-amyloid deposition in APP/PS1 double transgenic Alzheimer mice. Neurobiol Dis 18:134–142.

Moore S, Thanos S. 1996. The concept of microglia in relation to central nervous system disease and regeneration. Prog Neurobiol 48:441–460.

Naito M, Hasegawa G, Takahashi K. 1997. Development, differentiation, and maturation of Kupffer cells. Microsc Res Techniq 39:350–364.

Nakagawa T, Kim TS, Murai N, Endo T, Iguchi F, Tateya I, Yamamoto N, Naito Y, Ito J. 2003. A novel technique for inducing local inner ear damage. Hear Res 176:122–127.

Okabe M, Ikawa M, Kominami K, Nakanishi T, Nishimune Y. 1997. 'Green mice' as a source of ubiquitous green cells. FEBS Lett 407:313–319.

Okano T, Nakagawa T, Kita T, Endo T, Ito J. 2006. Cell-gene delivery of brain-derived neurotrophic factor to the mouse inner ear. Mol Ther (in press).

Olson JK, Miller SD. 2004. Microglia initiate central nervous system innate and adaptive immune responses through multiple TLRs. J Immunol 173:3916–3924.

Shiga A, Nakagawa T, Nakayama M, Endo T, Iguchi F, Kim TS, Naito Y, Ito J. 2005. Aging effects on vestibulo-ocular responses in C57BL/6 mice: comparison with alteration in auditory function. Audiol Neurootol 10:97–104.

Shinohara T, Bredberg G, Ulfendahl M, Pyykko I, Olivius NP, Kaksonen R, Lindstrom B, Altschuler R, Miller JM. 2002. Neurotrophic factor intervention restores auditory function in deafened animals. Proc Natl Acad Sci U S A 99:1657–1660.

Simard AR, Rivest S. 2004. Bone marrow stem cells have the ability to populate the entire central nervous system into fully differentiated parenchymal microglia. FASEB J 18:998–1000.

Streit WJ. 1996. The role of microglia in brain injury. Neurotoxicology 17:671–678.

Tornabene SV, Sato K, Pham L, Billings P, Keithley EM. 2006. Immune cell recruitment following acoustic trauma. Hear Res 222:115–124.

Xu H, Chen M, Mayer EJ, Forrester JV, Dick AD. 2007. Turnover of resident retinal microglia in the normal adult mouse. Glia 55:1189–1198.

Yoshimoto M, Shinohara T, Heike T, Shiota M, Kanatsu-Shinohara M, Nakahata T. 2003. Direct visualization of transplanted hematopoietic cell reconstitution in intact mouse organs indicates the presence of a niche. Exp Hematol 31:733–740.

Eur Arch Otorhinolaryngol
DOI 10.1007/s00405-008-0760-3

OTOLOGY

Efficiency of a transtympanic approach to the round window membrane using a microendoscope

Harukazu Hiraumi · Takayuki Nakagawa · Juichi Ito

Received: 12 March 2008 / Accepted: 1 July 2008

Abstract There has been increasing interest in cochlear drug delivery through the round window membrane (RWM). However, placing drugs on the RWM is difficult because of anatomical barriers. We examined the efficacy of a microendoscope for a transtympanic approach to the RWM. We evaluated the visibility of the RWM using four approaches: transtympanic microendoscopic, transtympanic microscopic, transmastoid microendoscopic, and transmastoid microscopic in ten human temporal bones. For the transtympanic approach, we made a fenestration (2 × 1 mm) in the postero-inferior quadrant of the tympanic membrane. For the transmastoid approach, conventional posterior hypotympanotomy was performed. The transtympanic microendoscopic approach enabled visualization of the RWM in all specimens, whereas the transtympanic microscopic approach only permitted visualization in three specimens. Through the transmastoid approach, the RWM was visible in all specimens using either a microendoscope or a microscope. The transtympanic microendoscopic approach can be utilized for cochlear drug delivery through the RWM.

Keywords Microendoscope · Round window membrane · Cochlea · Drug delivery

Introduction

Sensorineural hearing loss (SNHL) is one of the most common disabilities in industrial countries. Systemic administration of steroids has been widely used for the treatment of acute profound hearing loss [1]; however there are limitations in their clinical efficacy [2]. At present, therapeutic strategies are limited to hearing aids and cochlear implants for patients with chronic SNHL. Based on this background, basic investigations have elucidated several agents that are effective for the treatment of SNHL. However, the problem of how to deliver drugs to the inner ear has been a considerable obstacle to the development of treatments for SNHL. The blood-inner ear barrier prevents the transportation of serum drugs to the inner ear, and the blood flow to the inner ear is very limited.

Drug transduction through the round window membrane (RWM) is one option for delivering drugs into the inner ear. Continuous infusion of RWM with an osmotic pump and microcatheter has been reported as an effective and safe approach [3]. However, it requires surgery and the invasion cannot be overlooked. Recently, new local drug application procedures using biodegradable substances are gaining interest [4, 5]. The inner ear is one of the targets for local drug administration using biodegradable gelatin hydrogels [6, 7]. In this drug delivery system, positively charged proteins or peptides are electrostatically trapped in negatively charged gelatin polymer chains. As the gelatin polymer chains degrade, proteins or peptides are released from the hydrogel. The released protein is conveyed through the RWM into the inner ear via a concentration gradient. Therefore, close contact of biodegradable hydrogels with the RWM is critical for efficient drug delivery to inner ear fluids.

The RWM is situated perpendicular to the tympanic membrane and deep in the round window niche. In some cases, a false membrane covers the RWM. For safe and certain drug administration, hydrogels containing drugs should be placed on the RWM under direct visualization. Use of a

H. Hiraumi (✉) · T. Nakagawa · J. Ito
Department of Otolaryngology, Head and Neck Surgery,
Graduate School of Medicine, Kyoto University,
Kawaharacho 54, Shogoin, Sakyo-ku, 606-8507 Kyoto, Japan
e-mail: hhiraumi@ent.kuhp.kyoto-u.ac.jp

microendoscope is an effective method for visualization of the RWM [8]. It is equipped with a working channel, which can be used in drug administration. However, the potential of microendoscopes for placing substrates on the RWM has not been evaluated, and it is important to clarify the prevalence of subjects in whom the RWM is microendoscopically visible. In the present study, we examined the potential of a specially modified microendoscope for a transtympanic approach to the RWM using human temporal bones.

Materials and methods

Ten formalin-fixed temporal bones with no middle or inner ear diseases were obtained from six individuals (aged from 68 to 76 years at death, five male, and one female). A microendoscope (0.9 mm in outer diameter, 50 mm in length; FiberTech, Tokyo, Japan) was specially modified in the fit angle for observation of the RWM through the tympanic membrane. The tip is curved 15° (Fig. 1). The view angle is 70°. It is equipped with a working channel (0.3 mm in diameter).

We used four different approaches to observe the RWM as follows: (1) transtympanic microendoscopic, (2) transtympanic microscopic, (3) transmastoid microendoscopic, and (4) transmastoid microscopic. For the transtympanic approach, a small fenestration (2 × 1 mm) was made in the posterior inferior quadrant of the tympanic membrane using a knife (Fig. 2). The microendoscope was inserted into the middle ear through this fenestration and set to provide the best view of the RWM. For observation with a microscope, the fenestration edge in the tympanic membrane was gently pushed with a curved needle to obtain the best access to the RWM. For transmastoid approaches, canal-wall up complete mastoidectomy and posterior hypotympanotomy were performed under conventional microscopy (Leica M300, Leica Microsystems, Wetzlar, Germany). The bones covering the middle cranial fossa dura, the posterior fossa dura, and the sigmoid sinus were drilled to be as thin as possible. The bony wall of the external auditory canal was preserved. The facial nerve and chorda tympani nerve were skeletonized and the facial recess was opened as large as possible (Fig. 2).

Fig. 1 A microendoscope specially modified for better visualization of the RWM. The outer diameter is 0.9 mm and the length is 50 mm. The view angle is 70°. It is equipped with a working channel (0.3 mm in diameter)

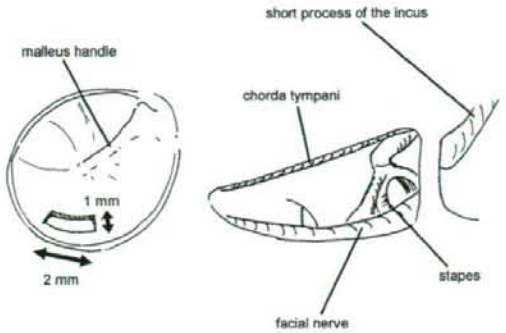

Fig. 2 A small fenestration (2 × 1 mm) was made in the posterior inferior quadrant of the tympanic membrane using a knife. Posterior hypotympanotomy was made as large as possible. In all specimens, the facial nerve and chorda tympani were skeletonized

The RWM was observed through a posterior hypotympanotomy with a microendoscope or a microscope. Surgical procedures were performed by one author (Harukazu Hiraumi). The view of the RWM and surrounding structures using the four approaches was video-captured. Frames showing best view of the RWM were converted into still images, and the area of the RWM was measured using image-processing program, ImageJ. An angled hook (1.0 mm sharp tip) was used as a reference. Total area of the RWM was measured after drilling the round window niche. The visibility of the RWM was calculated and graded into three classes: Grade I as no or little visualization of the RWM (<20%), Grade II as defined by >20%, and Grade III as defined by >70%. In three samples, the round window niche was covered with false membranes. In these cases, the false membranes were removed with a curved needle under microscopic view via posterior hypotympanotomy.

Results

A microendoscope was smoothly inserted into the middle ear cavity and the incuidostapedial joint was observed easily in all the specimens. The percentage of the area of the

RWM under direct vision was shown in the Table 1. The transtympanic microendoscopic approach enabled visualization of the RWM in all the specimens (Fig. 3). In three specimens, the RWM was totally observed (Fig. 4a). We used the incuidostapedial joint as a landmark to identify the location of the round window niche and the tip of the microendoscope was safely oriented to the RWM. No hazardous events such as ossicular dislocation or disruption of the tympanic membrane occurred. In contrast to the transtympanic microendoscopic approach, a transtympanic approach using a microscope provided visualization of the RWM in only three specimens (Fig. 3). Even in those three specimens, the view of the RWM was very limited (Fig. 4c). In the other seven specimens, the RWM was not observed, as the overhang of the round window niche was an obstacle for visualization. The visibility of the RWM through the transtympanic microendoscopic approach was significantly superior to that through transtympanic microscopic approach (Fig. 3, $P < 0.01$, Wilcoxon matched-pair signed-rank test).

In all the specimens, the transmastoid approach provided an excellent view of the RWM using either microendoscope (Fig. 4b) or microscope (Fig. 4d). The transmastoid microendoscopic approach provided a wide view of the middle ear cavity; for instance more than 70% of the tympanic membrane was visible in nine (microendoscopic), and seven (microscopic) specimens.

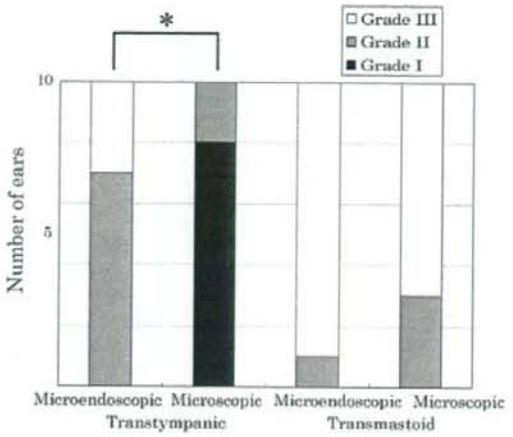

Fig. 3 The visibility of the RWM for four approaches. Grade I as no or little visualization of the RWM (<20%), Grade II as defined by >20%, and Grade III as defined by >70%. The visibility through the transtympanic microendoscopic approach was better than that with transtympanic microscopic approach

Discussion

The present results demonstrate that a microendoscope provided a satisfactory view of the RWM through a transtympanic approach with only a 2-mm incision on the tympanic membrane. Although the transmastoid microscopic approach provides an excellent view and favorable access to the RWM, this approach requires mastoidectomy and is not adequate for local drug application for treatment of SNHL. In contrast, the transtympanic microendoscopic approach requires only a small fenestration in the tympanic membrane. Therefore, the transtympanic microendoscopic approach may be applicable for office-based treatment.

Conventional endoscopes with 30° provide good visualization of the RWM [9, 10]. However, endoscopes with attached CCD cameras are not easy to handle. In office-based usage, the endoscope is usually placed just outside of the tympanic membrane [11], and tools used for drug application can hinder the view. The outer diameter is 1.7 mm or larger, requiring larger myringotomy. In addition, use of a conventional endoscope for drug delivery onto the RWM requires another channel for drug application, resulting in

Table 1 The percentage of the visible area of the round window membrane using four approaches

No	Side	Transtympanic		Transmastoid	
		Microendoscope (%)	Microscope (%)	Microendoscope (%)	Microscope (%)
1	Left	80.2	0.0	91.6	70.1
2	Left	54.5	0.0	78.1	72.0
3	Left	78.8	23.0	87.3	79.6
4	Left	59.1	0.0	73.3	84.8
5	Left	48.2	14.6	94.8	71.6
6	Right	49.7	0.0	80.7	61.3
7	Right	79.9	0.0	87.6	75.7
8	Right	39.5	0.0	66.2	42.3
9	Right	62.0	20.1	84.9	83.2
10	Right	56.9	0.0	82.8	65.4

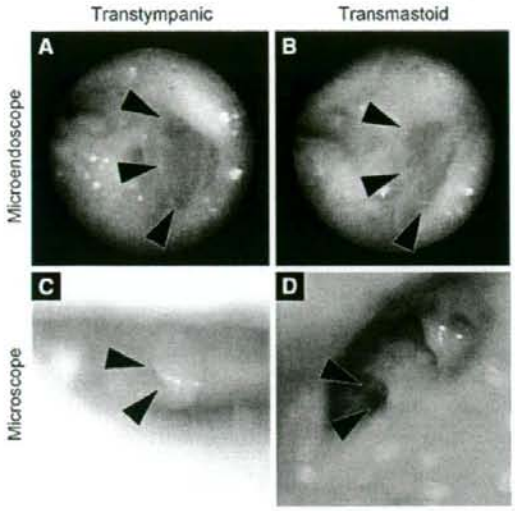

Fig. 4 The RWM of bone three observed through four approaches (*arrow heads*). The transtympanic microendoscopic approach (**a**), transmastoid microendoscopic approach (**b**), and transmastoid microscopic approach (**d**) provided good views. In the transtympanic microscopic approach (**c**), only a small part of the RWM was observed with the aid of a curved needle

increase of surgical invasion on the tympanic membrane. This means that enlargement of the size of tympanotomy or making additional tympanotomy site is necessary. Conventional microendoscopes are made for the inspection of the nasolacrymal ducts, and their tips are straight. The external auditory canal is S-shaped [12], and it is difficult to direct straight microendoscope to the RWM. The modified microendoscope used in the current study is quite smaller than conventional ones, and is connected to a CCD camera system via a cable. The curved tip fitted the external auditory canal. This configuration provides excellent handling of equipment for drug delivery. In addition, the microendoscope used in this study has a working channel that can be utilized for application of substrates onto the RWM.

The aim of the current study was to evaluate the accurate RWM drug application efficacy of a microendoscope with angles modified to ease RWM access. For clinical use of previously developed local drug delivery systems [3, 8], safe and stable visualization of the RWM through the tympanic membrane is necessary. In this manuscript, we compared the transtympanic microendoscopic approach with the transmastoid microscopic approach, since it is the most common procedure to access the RWM. The transmastoid microscopic approach is the most reliable approach for observation of the RWM, and additional removal of the round window niche enabled measurement of the total area of the RWM, which was indispensable for quantitative analysis in the present study. The view provided by a microendoscope is enough to deliver drugs or biomaterials incorporating drugs onto the RWM, although it is not satisfactory for precise surgical procedures. Previous studies have demonstrated the efficacy of biodegradable gelatin hydrogels for local application of brain-derived neurotrophic factor [6] and insulin-like growth factor 1 [7, 13]. The present findings resolve the problem of how to place a hydrogel onto the RWM in the clinic.

This study also found some drawbacks for this instrument. The resolution of the microendoscope is not as high as that of conventional microscopes, which may impede the differentiation of the false membrane from the RWM [14]. Sufficient understanding of the surgical anatomy of the middle ear is necessary for appropriate use of the microendoscope in drug delivery onto the RWM. However, we consider that refinement of the quality of view provided by microendoscopes may resolve this problem.

Conclusion

The transtympanic microendoscopic approach provided satisfactory visualization of the RWM through the tympanic membrane, indicating that the microendoscope is a useful tool for placing drugs or drug-containing materials onto the RWM.

Acknowledgements This study was supported by a Grant-in-Aid for Researches on Sensory and Communicative Disorders from the Japanese Ministry of Health, Labour and Welfare, by a Grant from Japanese Foundation for Research and Promotion of Endoscopy and by a Grant from Tinnitus Research Initiative.

Conflict of interest We do not have a financial relationship with the organization that sponsored the research.

References

1. Wilson WR, Byl FM, Laird N (1980) The efficacy of steroids in the treatment of idiopathic sudden hearing loss. A double-blind clinical study. Arch Otolaryngol 106:772–776
2. Conlin AE, Parnes LS (2007) Treatment of sudden sensorineural hearing loss: I. A systematic review. Arch Otolaryngol Head Neck Surg 133:573–581. doi:10.1001/archotol.133.6.573
3. Plontke SK, Zimmermann R, Zenner HP et al (2006) Technical note on microcatheter implantation for local inner ear drug delivery: surgical technique and safety aspects. Otol Neurotol 27:912–917. doi:10.1097/01.mao.0000235310.72442.4e
4. Jeong B, Bae YH, Lee DS et al (1997) Biodegradable block copolymers as injectable drug-delivery systems. Nature 388:860–862. doi:10.1038/42218
5. Tabata Y, Yamada K, Miyamoto S et al (1998) Bone regeneration by basic fibroblast growth factor complexed with biodegradable hydrogels. Biomaterials 19:807–815. doi:10.1016/S0142-9612(98)00233-6
6. Endo T, Nakagawa T, Kita T et al (2005) Novel strategy for treatment of inner ears using a biodegradable gel. Laryngoscope 115:2016–2020. doi:10.1097/01.mlg.0000183020.32435.59

7. Iwai K, Nakagawa T, Endo T et al (2006) Cochlear protection by local insulin-like growth factor-1 application using biodegradable hydrogel. Laryngoscope 116:529–533. doi:10.1097/01.mlg.0000200791.77819.eb
8. Plontke SK, Plinkert PK, Plinkert B et al (2002) Transtympanic endoscopy for drug delivery to the inner ear using a new microendoscope. Adv Otorhinolaryngol 59:149–155
9. Karhuketo TS, Puhakka HJ, Laippala PJ (1997) Endoscopy of the middle ear structures. Acta Otolaryngol Suppl 529:34–39. doi:10.3109/00016489709124074
10. Silverstein H, Rowan PT, Olds MJ et al (1997) Inner ear perfusion and the role of round window patency. Am J Otol 18:586–589
11. Kakehata S, Futai K, Kuroda R et al (2004) Office-based endoscopic procedure for diagnosis in conductive hearing loss cases using OtoScan Laser-Assisted Myringotomy. Laryngoscope 114:1285–1289. doi:10.1097/00005537-200407000-00027
12. Remley KB, Swartz JD, Harnsberger HR (1998) The external auditory canal. In: Swartz JD, Harnsberger HR (eds) Imaging of the temporal bone, 3rd edn. Thieme, New York, pp 16–20
13. Lee KY, Nakagawa T, Okano T et al (2007) Novel therapy for hearing loss: delivery of insulin-like growth factor 1 to the cochlea using gelatin hydrogel. Otol Neurotol 28:976–981
14. Schicker S (1957) Das runde Fenster. Laryngologie 36:149–153

Acta Oto-Laryngologica
2009, 1–5, iFirst article

informa
healthcare

ORIGINAL ARTICLE

Local application of hepatocyte growth factor using gelatin hydrogels attenuates noise-induced hearing loss in guinea pigs

TAKATOSHI INAOKA[1], TAKAYUKI NAKAGAWA[1], YAYOI S. KIKKAWA[1], YASUHIKO TABATA[2], KAZUYA ONO[1], MITSUHIRO YOSHIDA[1], HIROHITO TSUBOUCHI[3], AKIO IDO[3] & JUICHI ITO[1]

[1]*Department of Otolaryngology-Head and Neck Surgery, Graduate School of Medicine,* [2]*Department of Biomaterials, Field of Tissue Engineering, Institute for Frontier Medical Science, Kyoto University, Kyoto and* [3]*Department of Digestive and Life-style Related Diseases, Graduate School of Medical and Dental Sciences, Kagoshima University, Kagoshima, Japan*

Abstract

Conclusion: Local application of hepatocyte growth factor using biodegradable gelatin hydrogels attenuates noise-induced hearing loss in guinea pigs. *Objectives:* To develop an inner ear drug delivery system using gelatin hydrogels that is capable of a sustained delivery of growth factors to the cochlea. We examined the efficacy of the local application of gelatin hydrogels containing hepatocyte growth factor (HGF) in protecting cochlear hair cells from noise-induced damage. *Materials and methods:* A piece of gelatin hydrogel previously immersed in either HGF or saline was placed on the round window membrane of a guinea pig 1 h after noise exposure (4 kHz octave band noise at 120 dB sound pressure level for 3 h). Auditory function was monitored using auditory brainstem responses (ABRs), and the loss of hair cells was evaluated quantitatively. *Results:* Local HGF treatment significantly reduced the noise exposure-caused ABR threshold shifts and the loss of outer hair cells in the basal portion of the cochleae.

Keywords: *Cochlea, drug delivery, growth factor, protection, hair cell*

Introduction

Sensorineural hearing loss (SNHL) is one of the most common disabilities. However, available therapeutic options are limited to hearing aids and cochlear implants. Therefore, many investigations have concentrated on finding novel therapeutic molecules that could possibly be used in the treatment of SNHL. These studies have discovered several agents that exhibit therapeutic activity against SNHL. Despite such basic research progress, the translation of these basic findings into useful therapeutic clinical agents has yet to be achieved. One considerable obstacle to the development of such clinical applications revolves around the current lack of a safe and effective method for drug delivery to the cochlea. As a way of resolving this, we have developed a new method for local inner ear treatment that uses gelatin hydrogel as the inner ear drug delivery system [1]. Biodegradable gelatin hydrogel has been used previously for the sustained release of proteins or peptides, including growth and trophic factors [2]. We have previously demonstrated the efficacy of gelatin hydrogels in the sustained delivery of brain-derived neurotrophic factor [3] and insulin-like growth factor 1 (IGF-1) [4,5] in animal experiments. In addition, we are currently performing a clinical trial designed to examine local IGF-1 therapy that uses gelatin hydrogels for treating acute SNHL (http://www.kuhp.kyoto-u.ac.jp/~ent/ClinicalTrial/Gel_Eng.html).

Hepatocyte growth factor (HGF) was originally identified as the protein that is responsible for stimulating hepatocyte proliferation [6]. It is present in various cells and is a paracrine cellular growth and morphogenetic factor [7,8]. Hearing impairment caused by aminoglycosides is ameliorated after the transfer of the HGF gene to the inner ear via an

Correspondence: Takayuki Nakagawa MD PhD, Department of Otolaryngology-Head and Neck Surgery, Graduate School of Medicine, Kyoto University, Kawaharacho 54, Shogoin, Sakyo-ku, 606-8507 Kyoto, Japan. Tel: +81 75 751 3346. Fax: +81 75 751 7225. E-mail: tnakagawa@ent.kuhp.kyoto-u.ac.jp

(Received 18 September 2008; accepted 22 December 2008)

ISSN 0001-6489 print/ISSN 1651-2251 online
DOI: 10.1080/00016480902725197

intrathecal injection of the viral vector [9]. The HGF gene transfer for the treatment of SNHL has been published and patented (US Patent 7390482). Thus, local, sustained application of rhHGF might be effective for the treatment of SNHL and could potentially be approved for clinical applications in the near future.

Previous reports have documented the potential use of gelatin hydrogel for a sustained release of HGF [2,10]. Therefore, based on the previous reported data, we designed the current study to examine the efficacy of using gelatin hydrogels for local rhHGF application to treat noise-induced hearing loss (NIHL) in guinea pigs.

Materials and methods

Experimental animals

A total of 18 male 4-week-old adult Hartley guinea pigs weighing 300–350 g (Japan SLC, Hamamatsu, Japan) served as the experimental animals. Animal care was conducted under the supervision of the Institute of Laboratory Animals at the Kyoto University Graduate School of Medicine. All experimental procedures were performed in accordance with the National Institutes of Health Guidelines for the Care and Use of Laboratory Animals.

Biodegradable gelatin hydrogels

The biodegradable hydrogels were prepared as described previously [3–5]. Since other studies have analyzed the in vitro HGF release profiles from hydrogels and demonstrated that a hydrogel made with 10 mM glutaraldehyde allows for optimal HGF delivery [2,10], we designed the present study to use the same type of hydrogel.

Noise exposure and drug application

Baseline auditory brainstem response (ABR) thresholds were measured just before the noise exposure. Animals were then exposed to a 4 kHz octave band noise at 120 dB sound pressure level for 3 h in a ventilated sound exposure chamber. Sound levels were monitored and calibrated at multiple locations within the sound chamber to ensure stimulus uniformity.

A 2 mm^3 piece of hydrogel was immersed in 20 µl physiological saline that contained either 1.0 µg/µl rhHGF or physiologic saline alone (control). Under general anesthesia using midazolam (2 mg/kg, intramuscular; Astellas, Tokyo, Japan) and xylazine (2 mg/kg, intramuscular; Bayer, Tokyo, Japan), the piece of hydrogel was then placed on the round window membrane in the left ear of the animals 1 h after the noise exposure ($n = 6$ for each group).

Functional analysis

ABRs were measured to assess the auditory function, with the ABR threshold measurements performed at the 4, 8, and 16 kHz frequencies. ABRs were obtained before and after exposure to the noise, and on days 3, 7, 14, and 21 after the drug application. Animals were anesthetized using midazolam and xylazine and kept warm using a heating pad. Generation of acoustic stimuli and the recordings of the evoked potentials were performed using a PowerLab/4sp (AD Instruments, Castle Hill, Australia). Acoustic stimuli, consisting of tone-burst stimuli (0.1 ms cos^2 rise/fall with a 1 ms plateau), were delivered monaurally through a speaker (ES1spc; Bioresearch Center, Nagoya, Japan) that was connected to a funnel fitted to the external auditory meatus. To record bioelectrical potentials, subdermal stainless steel needle electrodes were inserted at the vertex (ground), ventrolateral to the measured ear (active) and contralateral to the measured ear (reference). Stimuli were calibrated against a ¼-inch free-field microphone (ACO-7016; ACO Pacific, Belmont, CA, USA) connected to an oscilloscope (DS-8812 DS-538; Iwatsu Electric, Tokyo, Japan) or a sound level meter (LA-5111; Ono Sokki, Yokohama, Japan). Responses between the vertex and mastoid subcutaneous electrodes were amplified using a digital amplifier (MA2; Tucker-Davis Technologies, Alachua, FL, USA). Thresholds were determined from a set of responses at varying intensities with 5 dB SPL intervals. Electrical signals were averaged for 1024 repetitions. Thresholds at each frequency were verified at least twice.

Histological analysis

On day 21 after the drug application, animals were deeply anesthetized with midazolam and xylazine and the cochleae were exposed. After removal of otic vesicles, 4% paraformaldehyde in 0.01 mol/l phosphate-buffered saline (PBS) at pH 7.4 was gently introduced into the perilymphatic space of the cochleae. Temporal bones were then excised and immersed in the same fixative at 4°C for 4 h. After rinsing with PBS, cochleae were dissected from temporal bones and subjected to histological analysis in whole mounts. To quantitatively assess the hair cell loss, we examined three regions of the cochlear sensory epithelia that were at a distance of 40–60%, 60–80% or 80–100% from the apex.

Immunohistochemistry for myosin VIIa and F-actin labeling by phalloidin were performed to label the surviving inner hair cells (IHCs) and outer hair cells (OHCs). Anti-myosin VIIa rabbit polyclonal antibody (1:500; Proteus Bioscience, Ramona, CA, USA) was used as the primary antibody, and Alexa-546-conjugated anti-rabbit goat IgG (1:500; Molecular Probe, Eugene, OR, USA) was used as the secondary antibody. Following immunostaining for myosin VIIa, specimens were then stained with FITC-conjugated phalloidin (1:300; Molecular Probe). Specimens were viewed under a confocal microscope (TCS SP2; Leica Microsystems, Wetzlar, Germany). To test the non-specific labeling, the primary antibody was omitted from the staining procedures. Three authors (T.I., T.N., and Y.S.K.) counted the numbers of IHCs and OHCs in 0.2 mm long regions of the apical, middle or basal portions of the cochleae. The average of the values was used as the data for each animal.

Statistical analysis

Overall effects of rhHGF application on ABR threshold shifts were examined using a two-way factorial analysis of variance. When interactions were significant, multiple comparisons with Fisher's protected least significant difference (PLSD) were used for pairwise comparisons. Differences in the IHC and OHC numbers for each region of the cochlea between the rhHGF- and saline-treated cochleae groups were examined using a Student's t test. Values of $p < 0.05$ were considered statistically significant. Values are expressed as the mean $\pm$ the standard error.

Results

Auditory function

Time courses of the alterations in the ABR threshold shifts at 4, 8, and 16 kHz after the application of rhHGF or saline are shown in Figure 1. Local application of rhHGF showed a significant effect on the reduction of the ABR threshold shifts at the 16 kHz frequency ($p = 0.030$). There was also a significant difference in threshold shifts on day 21 between the rhHGF- and saline-treated animals, as shown by the Fisher's PLSD test ($p = 0.045$). No significant differences were found for the threshold shifts between the two groups at 4 or 8 kHz.

Histological protection

Immunostaining for myosin VIIa and phalloidin staining demonstrated partial degeneration of the OHCs in the 60–80% distance regions from the apex

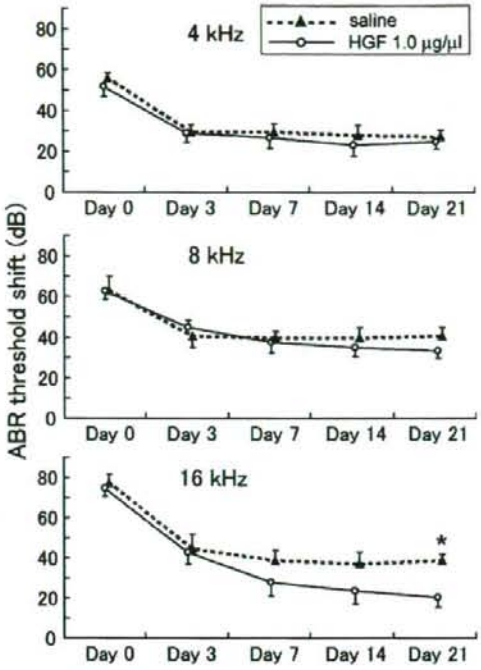

Figure 1. ABR threshold shifts after noise exposure in saline- and HGF-treated animals. An overall effect of HGF application is significant at 16 kHz (two factorial ANOVA, $p = 0.030$), not at 4 or 8 kHz. The difference in threshold shifts between saline- and HGF-treated animals is significant on day 21 at 16 kHz. *$p = 0.045$, Fisher's PLSD.

in the saline-treated cochleae (Figure 2A). The same region for the 1.0 μg/μl rhHGF-treated cochleae exhibited almost normal morphology (Figure 2B). In both experimental groups, OHC loss was not apparent in the 40–60% or 80–100% distance regions from the apex. IHCs were well maintained in every region of the cochleae in both groups. Quantitative assessments revealed a significant difference in OHC numbers in the 60–80% distance region from the apex between the saline- and rhHGF-treated cochleae (Figure 3, $p = 0.003$). No significant differences in OHC numbers were observed in the 40–60% or 80–100% distance regions. There were also no significant differences in the IHC numbers noted in any of the cochleae regions between the two experimental groups.

Discussion

Our findings indicate that local application of rhHGF using biodegradable gelatin hydrogels is effective in the attenuation of OHC damage due to noise trauma, resulting in the reduction of ABR

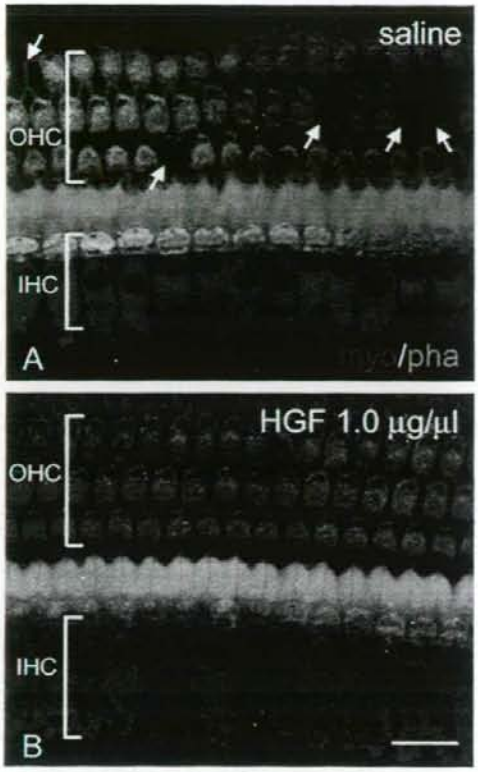

Figure 2. Immunostaining for myosin VIIa (myo) and phalloidin staining (pha) demonstrated loss of outer hair cells (OHC) in the upper basal portion of the saline-treated cochlea (A) and preservation of OHC in that of the HGF-treated cochlea (B). Arrows indicate loss of OHC. IHC, inner hair cells. Scale bar represents 20 μm.

thresholds. ABR measurements demonstrated that post-traumatic local application of rhHGF via gelatin hydrogels had a significant effect on the attenuation of threshold shifts at 16 kHz. Histological analyses demonstrated significant protection of the OHCs in the 60–80% distance from the apex, which is the region responsible for the 10–20 kHz hearing range [11].

Our previous study using IGF-1 indicated that there was a significant reduction of ABR threshold shifts at 4 or 8 kHz [9]. The present findings demonstrated that local HGF treatment caused significant effects at 16 kHz. The spread of the growth factors from the base to the apex of the cochlea occurred by diffusion. Thus, the molecular weights of growth factors could influence the distribution of these factors within the cochlea. The molecular weight of HGF is 69 kDa for the α-subunit and 34 kDa for the β-subunit, while that for

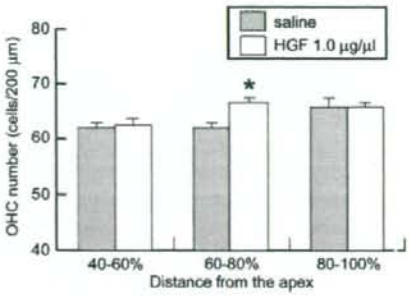

Figure 3. Means of numbers of surviving outer hair cells (OHCs) in saline- and HGF-treated cochleae. In the 60–80% distance region from the apex, the value of HGF-treated cochleae is significantly higher than that of saline-treated cochleae. *$p = 0.003$, t test. Bars represent standard errors.

IGF-1 is 7.6 kDa. Therefore, HGF may be abundantly distributed in the more basal portions of the cochlea as compared with that seen for the IGF-1 distribution.

Previous studies have demonstrated that several agents ameliorate NIHL when they are applied before noise exposure; however, only limited agents including IGF-1 [5] show protective effects by post-exposure administration. Local application of D-Jun N-terminal kinase-1 (D-JNK-1) peptide, an inhibitor of c-Jun N-terminal kinase, 12 h after noise exposure attenuates NIHL [12]. The efficacy of D-JNK-1 peptide has been demonstrated by application via an osmotic mini-pump or a hyaluronic acid gel. In the current study, we used the gelatin hydrogel for sustained delivery of rhHGF into the cochlea. This system may also be utilized for local delivery of D-JNK-1 peptide, because the gelatin hydrogel is suitable for sustained delivery of peptides [1,2]. The efficacy of local D-JNK-1 peptide application via gelatin hydrogels will be evaluated in the near future. Post-exposure administration of edaravone, a free radical scavenger, also rescues cochleae from NIHL [13]. Locally applied edaravone via an osmotic mini-pump can rescue OHCs even when it is applied 21 h after noise exposure. Edaravone is clinically available; however, how to deliver edaravone into the cochlea continuously is an obstacle for clinical use. Gelatin hydrogels are not suitable for sustained delivery of edaravone, because edaravone is not soluble in water [1,2]. Therefore, drug delivery systems that fit for edaravone should be developed before clinical application of local edaravone treatment.

The mechanisms of cochlear hair cell protection by HGF are not well understood. The cochlear hair cells are degraded through the process of apoptosis after exposure to intense noise [14]. Exposure to intense sound causes production of hydroxyl radicals

in the cochlear hair cells [15], which leads to peroxidation of the mitochondrial membrane and the release of cytochrome *c* from the mitochondria to the cytosol. The Bcl-2 family proteins, Bcl-xL and Bak, are produced in the hair cells following noise exposure, and it is the balance of these two proteins that is responsible for the regulation of this process [16]. Predominance of Bcl-xL, which is an anti-apoptotic member of the Bcl-2 family, results in the suppression of the cytochrome *c* release, whereas a predominance of the pro-apoptotic member, Bak, leads to the promotion of the cytochrome *c* release. HGF is known to up-regulate Bcl-xL, which is mediated by the phosphorylation of STAT3 [17]. Therefore, OHCs might be protected against noise through the same pathway. HGF also has anti-oxidant activity [18], which contributes to the protection of cells from apoptosis. This mechanism could possibly involve the same mechanism of protection provided by HGF for the OHCs. In the mechanisms of NIHL, disruption of afferent dendrites attached to IHCs is also involved [19]. Therefore, a regrowth of the nerve fibers and a re-afferentiation of the IHC is important for recovery of hearing after noise trauma. After spinal cord injury, HGF promotes axonal regrowth resulting in functional recovery [18]. This mechanism could also be involved in the significant reduction of ABR threshold shifts observed in the present study. In order to be able to elucidate the HGF distinct mechanism for the protection of auditory systems, further investigations are required.

In conclusion, the present findings suggest that HGF potentially has a role as a protector of OHCs from noise trauma. We are currently in the process of developing a clinical treatment for SNHL that administers local IGF-1 via gelatin hydrogels. Present results strongly suggest that HGF is the next therapeutic candidate that can be used as a local treatment agent via gelatin hydrogels in SNHL clinical trials.

Acknowledgements

This work was supported by a Grant-in-Aid for Research on Sensory and Communicative Disorders from the Japanese Ministry of Health, Labour and Welfare, and by a Grant-in-Aid for Scientific Research from the Ministry of Education, Culture, Sports, Science and Technology of Japan.

Declaration of interest: The authors report no conflicts of interest. The authors alone are responsible for the content and writing of the paper.

References

[1] Nakagawa T, Ito J. Drug delivery systems for the treatment of sensorineural hearing loss. Acta Otolaryngol Suppl 2007; 557:30–5.

[2] Young S, Wong M, Tabata Y, Mikos A. Gelatin as a delivery vehicle for the controlled release of bioactive molecules. J Control Release 2005;109:256–74.

[3] Endo T, Nakagawa T, Kita T, Iguchi F, Kim T, Tamura T, et al. Novel strategy for treatment of inner ears using a biodegradable gel. Laryngoscope 2005;115:2016–20.

[4] Iwai K, Nakagawa T, Endo T, Matsuoka Y, Kita T, Kim T, et al. Cochlear protection by local insulin-like growth factor-1 application using biodegradable hydrogel. Laryngoscope 2006;116:529–33.

[5] Lee K, Nakagawa T, Okano T, Hori R, Ono K, Tabata Y, et al. Novel therapy for hearing loss: delivery of insulin-like growth factor 1 to the cochlea using gelatin hydrogel. Otol Neurotol 2007;28:976–81.

[6] Gohda E, Tsubouchi H, Nakayama H, Hirono S, Sakiyama O, Takahashi K, et al. Purification and partial characterization of hepatocyte growth factor from plasma of a patient with fulminant hepatic failure. J Clin Invest 1988;81:414–9.

[7] Nakamura T, Nishizawa T, Hagiya M, Seki T, Shimonishi M, Sugimura A, et al. Molecular cloning and expression of human hepatocyte growth factor. Nature 1989;342:440–3.

[8] Funakoshi H, Nakamura T. Hepatocyte growth factor: from diagnosis to clinical applications. Clin Chim Acta 2003;327: 1–23.

[9] Oshima K, Shimamura M, Mizuno S, Tamai K, Doi K, Morishita R, et al. Intrathecal injection of HVJ-E containing HGF gene to cerebrospinal fluid can prevent and ameliorate hearing impairment in rats. FASEB J 2004;18:212–4.

[10] Ozeki M, Ishii T, Hirano Y, Tabata Y. Controlled release of hepatocyte growth factor from gelatin hydrogels based on hydrogel degradation. J Drug Target 2001;9:461–71.

[11] Viberg A, Canlon B. The guide to plotting a cochleogram. Hear Res 2004;197:1–10.

[12] Wang J, Ruel J, Ladrech S, Bonny C, van de Water TR, Puel JL. Inhibition of the c-Jun N-terminal kinase-mediated mitochondrial cell death pathway restores auditory function in sound-exposed animals. Mol Pharmacol 2007;71:654–66.

[13] Tanaka K, Takemoto T, Sugahara K, Okuda T, Mikuriya T, Takeno K, et al. Post-exposure administration of edaravone attenuates noise-induced hearing loss. Eur J Pharmacol 2005;522:116–21.

[14] Hu B, Guo W, Wang P, Henderson D, Jiang S. Intense noise-induced apoptosis in hair cells of guinea pig cochleae. Acta Otolaryngol 2000;120:19–24.

[15] Ohlemiller K, Wright J, Dugan L. Early elevation of cochlear reactive oxygen species following noise exposure. Audiol Neurootol 1999;4:229–36.

[16] Yamashita D, Minami S, Kanzaki S, Ogawa K, Miller J. Bcl-2 genes regulate noise-induced hearing loss. J Neurosci Res 2008;86:920–8.

[17] Nakagami H, Morishita R, Yamamoto K, Taniyama Y, Aoki M, Matsumoto K, et al. Mitogenic and antiapoptotic actions of hepatocyte growth factor through ERK, STAT3, and AKT in endothelial cells. Hypertension ;37(2 Part 2001;2): 581–6.

[18] Kitamura K, Iwanami A, Nakamura M, Yamane J, Watanabe K, Suzuki Y, et al. Hepatocyte growth factor promotes endogenous repair and functional recovery after spinal cord injury. J Neurosci Res 2007;85:2332–42.

[19] Ruel J, Wang J, Rebillard G, Eybalin M, Lloyd R, Pujol R, et al. Physiology, pharmacology and plasticity at the inner hair cell synaptic complex. Hear Res 2007;227:19–27.

JARO (2008)
DOI: 10.1007/s10162-008-0147-6

JARO
Journal of the Association for Research in Otolaryngology

A Mouse Model for Degeneration of the Spiral Ligament

SHINPEI KADA, TAKAYUKI NAKAGAWA, AND JUICHI ITO

[1]*Department of Otolaryngology, Head and Neck Surgery, Graduate School of Medicine, Kyoto University, 54 Kawaharacho, Shogoin, Sakyo-ku, Kyoto, 606-8507, Japan*

Received: 19 June 2008; Accepted: 27 October 2008

ABSTRACT

Previous studies have indicated the importance of the spiral ligament (SL) in the pathogenesis of sensorineural hearing loss. The aim of this study was to establish a mouse model for SL degeneration as the basis for the development of new strategies for SL regeneration. We injected 3-nitropropionic acid (3-NP), an inhibitor of succinate dehydrogenase, at various concentrations into the posterior semicircular canal of adult C57BL/6 mice. Saline-injected animals were used as controls. Auditory function was monitored by measurements of auditory brain stem responses (ABRs). On postoperative day 14, cochlear specimens were obtained after the measurement of the endocochlear potential (EP). Animals that were injected with 5 or 10 mM 3-NP showed a massive elevation of ABR thresholds along with extensive degeneration of the cochleae. Cochleae injected with 1 mM 3-NP exhibited selective degeneration of the SL fibrocytes but alterations in EP levels and ABR thresholds were not of sufficient magnitude to allow for testing functional recovery after therapeutic interventions. Animals injected with 3 mM 3-NP showed a reduction of around 50% in the EP along with a significant loss of SL fibrocytes, although degeneration of spiral ganglion neurons and hair cells was still present in certain regions. These findings indicate that cochleae injected with 3 mM 3-NP may be useful in investigations designed to test the feasibility of new therapeutic manipulations for functional SL regeneration.

Correspondence to: Takayuki Nakagawa · Department of Otolaryngology, Head and Neck Surgery, Graduate School of Medicine · Kyoto University · 54 Kawaharacho, Shogoin, Sakyo-ku, Kyoto, 606-8507, Japan. Telephone: +81-75-7513346; fax: +81-75-7517225; email: tnakagawa@ent.kuhp.kyoto-u.ac.jp

Keywords: 3-nitropropionic acid, endocochlear potential, cochlea, gap junction, Na, K-ATPase, fibrocyte

INTRODUCTION

Sensorineural hearing loss (SNHL) is a common disability in industrialized countries. Recent studies using human temporal bones and animal models have highlighted the importance of the spiral ligament (SL) in the pathogenesis of SNHL. Degenerative changes of the SL have been observed in human temporal bones with acoustic neuroma (Mahmud et al. 2003), endolymphatic hydrops (Vasama and Linthicum 1999), or presbycusis (Kusunoki et al. 2004; Ohlemiller 2004). Several animal models have also indicated the involvement of SL degeneration in the mechanisms for SNHL that are related to aging (Hequembourg and Liberman 2001; Spicer and Schulte 2002) or excessive noise (Hirose and Liberman 2003). The SL is located in the cochlear lateral wall and is composed of fibrocytes. The fibrocytes in the SL form a gap junction network, which is closely related to the maintenance of the endocochlear potential (EP; Xia et al. 1999). In addition, a recent study has indicated that the cochlear gap junctions also play a role in the transport of energy and nutrient supplies (Zhao 2005). A mouse model for DFN3, an X-chromosome-linked non-syndromic mixed deafness, exhibits a significant reduction in the immunoreactivity for the gap junction protein, connexin 26 (Cx26), in the SL fibrocytes, which results in a profound hearing loss (Minowa et al. 1999; Xia et al. 2002). Therefore, during SNHL treatment, the SL fibrocytes should be viewed as therapeutic targets.

Published online: 11 February 2009

Treatment options for SNHL are currently limited to cochlear implants and hearing aids. Thus, there is a need for the development of alternative means of biological therapy, such as cell and/or gene therapy. In fact, recent studies have demonstrated the potential of cell and/or gene therapy for the treatment of SNHL (Izumikawa et al. 2005; Okano et al. 2005, 2006). Such therapeutic strategies may be applicable for the regeneration of SL fibrocytes. However, in order to examine the efficacy of such novel therapeutic strategies for the regeneration of SL fibrocytes, an appropriate model for SL degeneration is required. Recently, a rat model for the selective loss of SL fibrocytes has been reported (Hoya et al. 2004; Okamoto et al. 2005). In this model, a direct application of 3-nitropropionic acid (3-NP) onto the round window membrane causes damage to the SL fibrocytes. 3-NP is an inhibitor of succinate dehydrogenase, an enzyme of the citric acid cycle on the mitochondria. However, in a series of rat experiments, EPs have not been evaluated, although the measurement of the EP is crucial for the evaluation of SL function. To this end, the aim of the present study was to establish a mouse model for selective loss of SL fibrocytes that also exhibited a significant reduction of the EP, which would make it possible to use this model as the basis for the development of therapeutic strategies for SL regeneration. We injected 3-NP into the posterior semicircular canal (PSCC) of C57BL/6 mice and monitored the cochlear function using measurements of auditory brain responses (ABRs) and EPs, followed by subsequent histological analyses of the cochleae.

METHODS

Animals

Female C57BL/6 mice (Japan SLC Inc., Hamamatsu, Japan) aged 6–10 weeks (n=59) were used as experimental animals. All of the animals were maintained at the Institute of Laboratory Animals, Kyoto University Graduate School of Medicine, Japan. The experimental protocols were approved by the Animal Research Committee of Kyoto University Graduate School of Medicine and were conducted in accordance with the US National Institutes of Health Guidelines for the Care and Use of Laboratory Animals.

Experimental groups

3-NP (Sigma, St. Louis, MO, USA) was dissolved into physiological saline at a concentration of 1, 3, 5, or 10 mM and adjusted to pH 7.4 with NaOH. We divided the experimental animals into four groups according to the applied concentration of 3-NP (1 mM, n=13; 3 mM, n=14; 5 mM, n=12; 10 mM, n=12). Animals administered physiological saline were used as controls (n=12).

3-NP administration

We used an injection of 3-NP into the semicircular canal as a method for drug application into the mouse cochlea, similar to previously reported studies (Nakagawa et al. 2003; Lee et al. 2003; Iguchi et al. 2004; Okano et al. 2006). This method makes it possible to administer drugs or place cell transplants into the cochlear fluid spaces without functional and/or histological damage to the cochlea. Under general anesthesia with midazolam (10 mg/kg), medetomidine (37.5 μg/kg) and butorphanol tartrate (0.5 mg/kg), a retroauricular incision was made in the left ear, and the PSCC was exposed. A small hole was then made in the bony wall of the PSCC. Using microscopy, a fused silica glass needle (Eicom, Kyoto, Japan) was then inserted into the perilymphatic space of the PSCC, and substrates were injected at a rate of 0.5 μl/min for 3 min using a microsyringe pump (Eicom). Thereafter, the hole was plugged with a fat graft and covered with fibrin glue. The animals that showed ABR threshold shifts less than 30 dB at the frequency of 40 kHz 1 day after 3-NP application were eliminated from experiments. One animal was eliminated from the 1 or 3 mM 3-NP group, and two animals were eliminated from the 5 mM 3-NPgroup.

ABR recording

An ABR recording was used to monitor the auditory function of the experimental animals. The right cochleae were mechanically destroyed in order to avoid cross hearing. Under general anesthesia, ABR measurements were performed as has been previously described (Shiga et al. 2005). The generation of acoustic stimuli and the subsequent recording of the evoked potentials were performed using a PowerLab/4sp (AD Instruments, Castle Hill, Australia). The acoustic stimuli, consisting of tone burst stimuli (0.1-ms cos2 rise/fall and 1-ms plateau) were delivered monaurally through a speaker (ES1spc, Bioresearch Center, Nagoya, Japan), which was connected to a funnel that was fitted into the external auditory meatus. In order to record the bioelectrical potentials, subdermal stainless steel needle electrodes were inserted at the vertex (ground), ventrolateral to the measured ear (active) and contra-lateral to the measured ear (reference). The stimuli were calibrated against a 0.25-in. free-field mike (ACO-7016, ACO Pacific Inc., Belmont, CA, USA) that was connected to an oscilloscope (DS-8812 DS-538, Iwatsu Electric, Tokyo, Japan) or a sound level meter (LA-5111, Ono

Sokki, Yokohama, Japan). The responses between the vertex and the mastoid subcutaneous electrodes were amplified with a digital amplifier (MA2, Tucker-Davis Technologies, Alachua, FL, USA). The ABRs were recorded before drug application and on postoperative days (PODs) 1, 7, and 14. Thresholds were determined for the frequencies of 10, 20, and 40 kHz from a set of responses at varying intensities with 5-dB SPL intervals. When no response was present at the highest sound level available, the threshold was designated as being 5 dB greater than that level so that statistical tests could be done.

Measurement of endocochlear potentials

EP recording was performed under general anesthesia on POD 14. A silver–silver chloride reference electrode was placed under the skin of the dorsum. An incision was then made in the inferior portion of the left postauricular sulcus, with the bulla perforated in order to allow for exposure of the stapedial artery and the basal turn of the cochlea. Thinning of the bone over the SL followed by the creation of a small opening with a pick made it possible to access to the scala media of the basal turn. A micropipette electrode (10–40 MO) filled with 150 mM KCl was advanced through the bony aperture into the SL. The entry of the electrode tip into the endolymph was characterized by fast changes of the recorded potentials. The electrode was advanced until a stable potential was observed. At the point of the stable potential, there were no alterations that were dependent upon the electrode depth. The signal was amplified through an amplifier (Duo 773, World Precision Instruments, Sarasota, FL, USA). As the electrode was advanced, the DC potentials were recorded via an A-D converter (PowerLab 4sp, AD Instruments) coupled to a desktop computer.

Tissue preparation

On POD 14, after measurements of EPs, the animals were deeply anesthetized with a lethal dose of anesthetic drugs followed by intracardial perfusion with physiological saline. Subsequently, 4% paraformaldehyde in 0.01 M phosphate-buffered saline (PBS) at pH 7.4 was infused. To decalcify the excised temporal bones, they were immersed in the same fixative at 4°C for 4 h and then placed into 0.1 M ethylenediaminetetraacetic acid in PBS. The number of sample subsets used for the evaluation of the hair cell damage in the whole mounts included control, n=4; 1 mM, n=4; 3 mM, n=5; 5 mM, n=4; and 10 mM, n=4. Remaining samples were utilized for morphometric analysis of frozen sections (n=8; 1, 3, 10 mM, n=6; 5 mM). Samples were embedded in OCT compound (Tissue-Tek, Sakura Finetechnical, Tokyo, Japan) and frozen at −80°C. For histological analysis, 10-μm-thick mid-modiolar sections of the cochleae were obtained and then prepared.

Immunohistochemistry

Immunohistochemistry for Na,K-ATPase α and Cx26 were employed in order to determine the sites that were affected by the local 3-NP application in the cochlear lateral wall. The primary antibodies were mouse anti-Cx26 antibody (1:500; Zymed Laboratories, South San Francisco, CA, USA) and rabbit monoclonal anti-Na, K-ATPase α antibody (1:500; Epitomics, Inc., Burlingame, CA, USA). Alexa-488 conjugated anti-rabbit goat IgG (1:500; Molecular Probes, Eugene, OR, USA) and Alexa-568 conjugated anti-mouse goat IgG (1:500; Molecular Probes) were used as the secondary antibodies.

Immunohistochemistry for βIII-tubulin (TuJ1) was performed to identify the spiral ganglion neurons (SGNs) in the Rosenthal's canal. The primary antibody was rabbit anti-βIII-tubulin antibody (1:250; Covance Research Products, Berkeley, CA, USA), and Alexa-568 conjugated anti-rabbit goat IgG (1:500; Molecular Probes) was used as the secondary antibody followed by nuclear staining with 4′,6-diamidino,2-phenylindole dihydrochloride (DAPI; 1 μg/ml in PBS; Molecular Probes).

Immunohistochemistry for myosin VIIa and F-actin staining by phalloidin were performed to identify cochlear hair cells or the locations in which hair cells were present in whole mounts. The primary antibody was rabbit anti-myosin VIIa antibody (1:500; Proteus Bioscience, Ramona, CA, USA), with Alexa-568 conjugated anti-rabbit goat IgG (1:500; Molecular Probes) used as the secondary antibody. Samples were then stained using fluorescein-isothiocyanate-conjugated phalloidin (3 μg/ml; Sigma-Aldrich, Inc.).

Quantitative assessments for histological damage

Morphometric assessments of the SL, the stria vascularis (SV) and the SGNs were performed for each cochlear turn as has been previously described (Suzuki et al. 2006). The sections stained with hematoxylin–eosin (HE) were used for the SL and the SV, and those stained by immunohistochemistry for βIII tubulin were used for the SGN. The cochlear specimens were observed using a light microscope (Olympus BX50, Tokyo, Japan). The images were acquired with a CCD camera connected to a personal computer. The areas of the SL, the SV, Rosenthal's canal, and the cochlear turn were quantified by measuring their cut surfaces using ImageJ software (http://www.nist.gov/lispix/imlab/prelim/dnld.

html). The total numbers of nuclei in the SL were counted for each cochlear turn. For the SGN, βIII tubulin- and DAPI-positive cells were counted. The cell density of the SL (SL density) and the SGN (SG density) and the ratio of the SV area (SV ratio) were used to reduce the variance caused by differences in the cutting directions among the cochlear specimens. The SL density was determined as the number of cell nuclei per 1 μm^2 of the SL area, and the SG density was determined as the number of cell nuclei per 1 μm^2 of Rosenthal's canal. The SV ratio was determined by dividing the SV area by that of the cochlear turn. We calculated the SL density, the SG density, and the SV ratio in two mid-modiolar sections separated by 40–50 μm from each cochlea, with the average defined as the data for the animal.

To reveal details of SL degeneration, a loss of five types of SL fibrocytes was examined, respectively. The types of SL fibrocytes were classified into type I–V fibrocytes according to their location in the SL (Spicer and Schulte 1991; Schulte and Steel 1994; Xia et al. 1999; Hirose and Liberman 2003). The density for each type was determined as the number of cell nuclei per square micrometer of the SL area.

Quantitative analyses for the numbers of remaining inner hair cells (IHCs) and outer hair cells (OHCs) were performed on whole mounts. The 20–40% distance portions from the apex were defined as being apical, the 40–60% distance portions were defined as upper basal, and the 60–80% distance portions were defined as basal. The numbers of IHCs and OHCs were counted in a 0.2-mm-long region of the apical, the upper basal, and the basal portion of the cochleae.

Statistical analyses

The overall effect on ABR threshold shifts of the local 3-NP applications was examined by a two-way factorial analysis of variance (ANOVA). When the interaction was significant, multiple comparisons with the Tukey–Kramer test were performed for pairwise analyses. Differences between the recorded time points for the EP, the SL or SG density, or the SV ratio among the experimental groups and in ABR thresholds in the control animals were examined by a single factorial ANOVA with the Scheffe's test. A p value less than 0.05 was considered statistically significant. All data are represented as the mean±standard error.

RESULTS

ABR threshold shift

In the control animals that were treated with saline, no significant elevations of the ABR thresholds were observed for any of the frequencies. In the experimental animals, local 3-NP applications of each of the concentrations used in this study caused significant ABR threshold shifts in a dose-dependent manner (Fig. 1A–C). The animals injected with 5 or 10 mM 3-NP exhibited approximately 80- to 90-dB threshold shifts on POD 1, with no recovery of the ABR thresholds noted during the observation period. The animals injected with 3 mM 3-NP showed a remarkable threshold shift on POD 1 that was similar to the 5 or 10 mM model, although there was a trend for recovery of the ABR threshold over time. The differences in the ABR threshold shifts between POD 1 and POD 7 or 14 were significant at 10 and 20 kHz. On POD 14, the 3 mM model exhibited significant threshold shifts for each of frequencies tested (50.4± 3.0 dB at 10 kHz, 56.2±2.9 dB at 20 kHz, 61.9±2.9 dB at 40 kHz). The animals injected with 1 mM 3-NP showed significant threshold shifts on POD 1, while on POD 14, the ABR thresholds at 10 and 20 kHz had returned to levels that were seen for the control animals (Fig. 1A,B). A significant ABR threshold shift (22.9±5.2 dB) was only found at 40 kHz on POD 14 in the animals injected with 1 mM 3-NP (Fig. 1C).

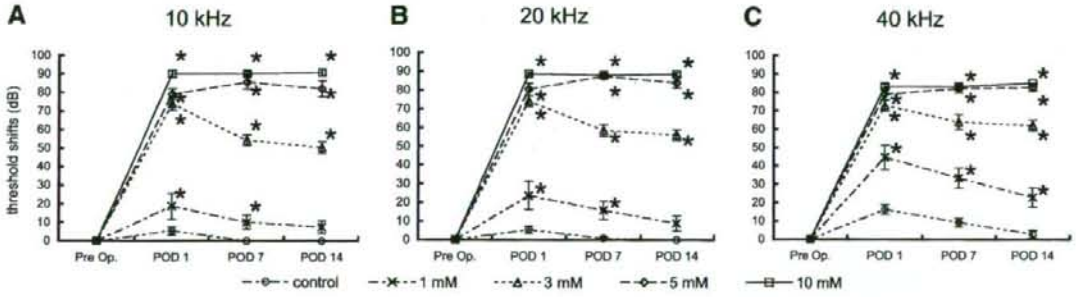

FIG. 1. Means of ABR threshold shifts at 10 (**A**), 20 (**B**), and 40 kHz (**C**) following local saline or 3-NP application on postoperative days (*POD*) 1, 7, and 14. Local applications of 3-NP have significant interactions with threshold shifts at all the frequencies ($p<0.0001$, two-way factorial ANOVA). *Asterisks* indicate significant differences to the control group in threshold shifts by multiple comparisons with the Tukey–Kramer test. *Bars* represent standard errors.

Endocochlear potentials

The mean value of the EPs for the control animals that were treated with saline was 110.5±2.4 mV. Local application of 3-NP induced a dose-dependent decrease of the EP levels, with the overall effect of the 3-NP application on the EP levels found to be statistically significant (Fig. 2). In the animals injected with 5 or 10 mM 3-NP, the EP levels decreased to almost undetectable levels (Fig. 2). In animals injected with 3 mM 3-NP, there was a significant decrease of the EP levels to approximately 50% of that seen in the control animals (56.4±3.7 mV, $p<0.0001$; Fig. 2). The animals injected with 1 mM 3-NP also exhibited a significant decrease of the EP levels (92.3± 1.5 mV, $p=0.005$; Fig. 2).

Degeneration of the spiral ligament

Figure 3 shows low magnification images of cochlear sections stained by HE and immunohistochemistry for Na,K-ATPase α in each experimental group. In cochleae injected with 1 mM 3-NP, a loss of fibrocytes was noted in the inferior portion of the SL in the basal and upper basal portions of cochleae (Fig. 3C). Immunohistochemistry for Na,K-ATPase α also demonstrated a decrease of immunoreactivity in the inferior portion of the SL in the upper basal and basal portions of cochleae (Fig. 3D). A loss of SL fibrocytes was also found in the lower basal portion of cochleae similarly to the basal portion. Degeneration in the SL and the SGN progressed depending on the concentration of 3-NP. Cochlear specimens damaged by 3 mM 3-NP exhibited SGN degeneration in the apical and the upper basal portions of cochleae (Fig. 3E). In cochleae injected with 5 mM 3-NP, a loss of fibrocytes and a decrease of immunoreactivity for Na,K-ATPase α extended to the superior portion of the SL (Fig. 3G–J). In addition, a significant loss of SGNs was observed in each turn of cochleae in specimens damaged by 10 mM 3-NP (Fig. 3I). A quantitative analysis of the SL density revealed dose-dependent decreases of the SL density by the local 3-NP applications in every portion of the cochleae (Fig. 4A). In addition, a loss of SL fibrocytes increased in a gradient from the apical to the basal portion of the cochlea.

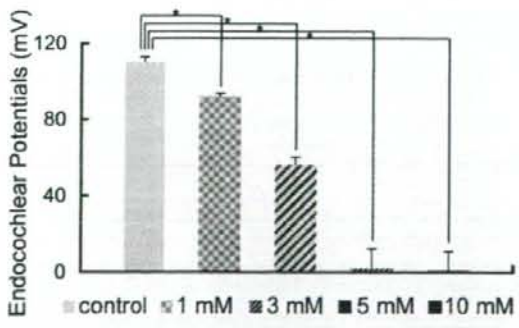

FIG. 2. Means of the endocochlear potentials (*EPs*) in the cochleae following local saline or 3-NP application. Local 3-NP application induces the significant and dose-dependent decrease of the EPs ($p<0.0001$, ANOVA). *Asterisks* indicate significant differences to the control group at $p<0.05$ (ANOVA with the Scheffe's test). *Bars* represent standard errors.

Alterations in cell densities of type I–V fibrocytes areas after the local 3-NP application are shown in Figure 4B–F, respectively. No significant decreases of cell densities in the type I area were found in each portion of cochleae. For the type II area, significant decreases of cell densities were observed in each portion of cochleae in a dose-dependent manner (Fig. 4C). A loss of fibrocytes in the type II area was most prominent in the basal portion of cochleae. Only the type II area demonstrated a significant loss in the apical portion of cochleae injected with 1 mM 3-NP. The type III–V areas also showed significant decreases of cell densities in each portion of cochleae in a dose-dependent manner (Fig. 4D–F). In these areas of the SL, degeneration of SL fibrocytes also increased in gradient from the apical to the basal portion of the cochlea.

Immunohistochemistry for Cx26 and Na,K-ATPase α demonstrated an alteration in the distribution of their expression in the SL following local 3-NP application. In the control cochleae that were treated with physiological saline, expression of Cx26 was observed in the SL. Strong immunoreactivity was found in the superior portion of the SL, while moderate immunoreactivity was noted in the inferior portion (Fig. 5A). The SV and the inferior portion of the SL exhibited strong expression of Na,K-ATPase α, and the middle portion of the SL showed a weak or moderate immunoreaction for Na,K-ATPase α (Fig. 5E). In the cochleae that were damaged by all concentrations of 3-NP, immunoreactivity for Cx26 was either absent or faint in the inferior portion of the SL, while its expression was still observed in the superior portion of the SL (Figs. 5B–D). In the cochleae damaged by 1 or 3 mM of 3-NP, a decrease in the immunoreactivity for Na,K-ATPase α was found in the inferior portion of the SL (Figs. 4F–H). The immunoreactivity was absent in the inferior portion of the SL in cochleae that were damaged by 5 (Fig. 5H) or 10 mM. Qualitative findings in immunohistochemistry were identical to the findings in quantitative analyses of cell densities in type I fibrocytes, which are located in the middle and superior portions of the SL and express Cx26 (Xia et al. 1999), and type II fibrocytes, which are located in the inferior portion of the SL and express